Material characterisation for optical wireless communication combining measurement and Monte Carlo simulations

Pierre Combeau, Lilian Aveneau, Pierre Thuillier Le Gac, Ruqin Xiao

IET Optoelectronics

Special Issue Call for Papers

Be Seen. Be Cited.
Submit your work to a new IET special issue

Connect with researchers and experts in your field and share knowledge.

Be part of the latest research trends, faster.

Read more

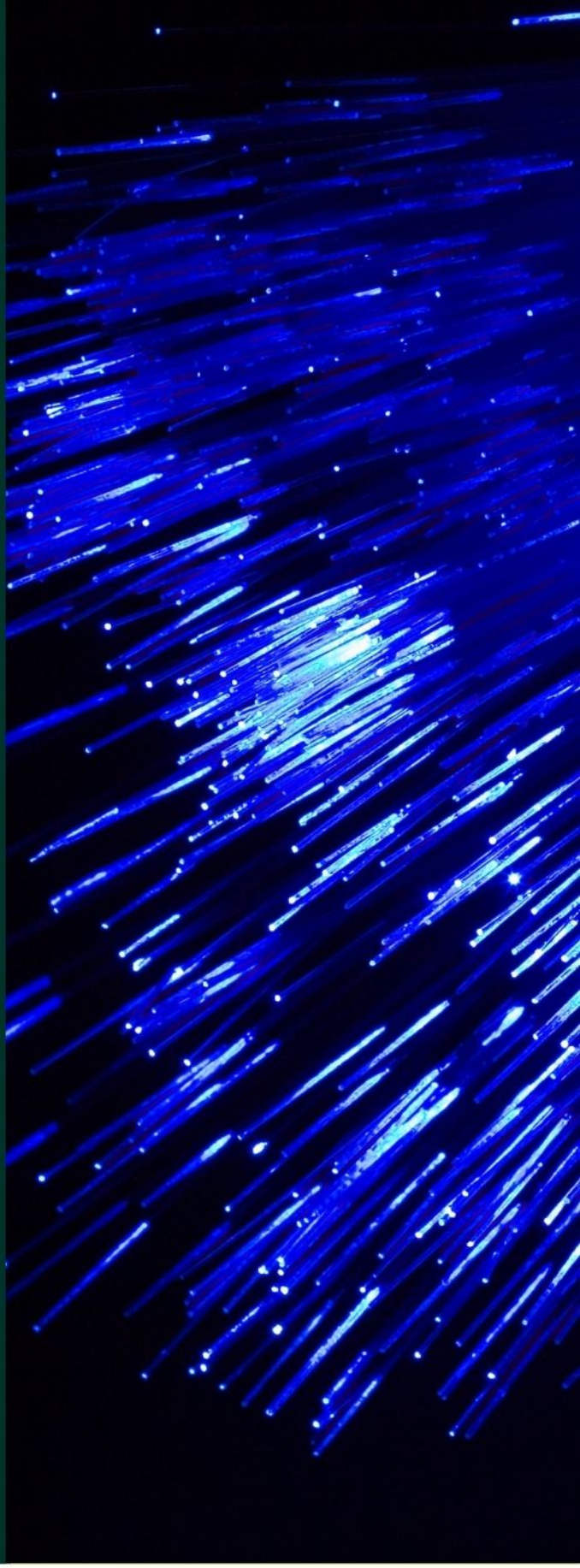

The Institution of Engineering and Technology

Received: 4 February 2023 | Revised: 3 May 2023 | Accepted: 8 June 2023

IET Optoelectronics

DOI: 10.1049/ote2.12098

The Institution of Engineering and Technology WILEY

ORIGINAL RESEARCH

Material characterisation for optical wireless communication combining measurement and Monte Carlo simulations

Pierre Combeau | **Lilian Aveneau** | **Pierre Thuillier Le Gac** | **Ruqin Xiao**

XLIM Laboratory, UMR CNRS 7252, University of Poitiers, Poitiers, France

Correspondence

Pierre Combeau, 11 bd Marie et Pierre Curie, TSA41123, Poitiers Cedex 9 86073, France.
Email: pierre.combeau@univ-poitiers.fr

Funding information

European Union, Grant/Award Number: 737645; Nouvelle-Aquitaine Region, Grant/Award Number: 8554510

Abstract

A method is proposed for optical characterisation of materials, which is a very important input for realistic channel simulation based on Monte-Carlo Ray-Tracing algorithms. This original approach consists first of all in carrying out some measurements of the optical power received after propagation in the environment containing the materials sought, using a simple and low-cost experimental setup. In a second step, this approach is based on an optimization algorithm. It takes as input the optical power measurements made, associated with the parameters of the measurement environment, such as the positions or properties of the sensors. This algorithm searches for the parameters of the material reflection models, minimising the difference between the optical measurement and the simulation. Two cost functions are studied to perform this search and showed that the correlation measure is the more robust one. To avoid uncertainties in the real input data, this approach is discussed using only a virtual configuration with well-controlled input data and thus a virtual measurement obtained by simulation. The results show that this method produces a correct estimate of the Bidirectional Reflectance Distribution Function (BRDF) albedos, provided that the chosen BRDF models correspond well to the reflection behaviour of the materials, and that the materials have a significant influence on the measured optical power.

KEYWORDS

genetic algorithms, Monte Carlo methods, optical communication, optical materials, reflectivity

1 | INTRODUCTION

Optical Wireless Communication (OWC) is a promising technology constituting an alternative or a complementary solution for future wireless radio-frequency networks, especially in indoor environments with Visible Light Communication (VLC) systems [1–3]. The main interest of VLC is to add a new wireless communication capability to lighting devices. Furthermore, OWC also offers numerous advantages, including immunity to electromagnetic interference, enhanced transmission security and a large unregulated bandwidth.

To evaluate communication performance in OWC context, the mainly used tools are based on Monte-Carlo Ray-Tracing (MCRT) algorithms, which, from a 3D geometrical model of the propagation environment, the optical characteristics of emission and reception sensors and the optical properties of the materials compute the line-of-sight (LOS) and multi-reflected contributions between the source and the receiver [4] to assess the propagation channel in realistic environments. The 3D environment can be easily modelled with a low set of surfaces for very simple configurations [5] or with Computer-Aided Design tools in case of more complex geometry [6]. The radiation patterns of optical sources can be modelled by simple analytical models as the conventional Generalised Lambertian one [7] or by experimental datasets provided by numerical simulation or measurement [8].

The Bidirectional Reflectance Distribution Function (BRDF) models the reflection properties of materials [9]. It is defined at a surface point x with local normal vector $\vec{n}$ as the

ratio between the reflected radiance $dL_r(x, \overrightarrow{\omega_r})$ in direction $\overrightarrow{\omega_r}$ over the received radiance $L_i(x, \overrightarrow{\omega_i})$ from direction $\overrightarrow{\omega_i}$:

$$R(x, \overrightarrow{\omega_i}, \overrightarrow{\omega_r}) = \frac{dL_r(x, \overrightarrow{\omega_r})}{L_i(x, \overrightarrow{\omega_i}) |\overrightarrow{\omega_i} \cdot \overrightarrow{n}| d\overrightarrow{\omega_i}}. \quad (1)$$

Hence, it gives the spatial distribution of the reflected optical power. The conventional Lambertian model is the most used BRDF in the literature. Given as a constant value corresponding to the surface's albedo, it models a perfectly diffuse surface.

Unfortunately, the albedo values are poorly known and only a few set of data are provided in the literature for only some materials and wavelengths [10–13]. These fragmentary data are not sufficient to describe all materials that appear into all possible simulation environments. Furthermore, it was showed in Refs [14, 15] that reflection properties of materials can significantly impact the communication performance, especially with low albedo. Therefore, in the context of OWC, the optical characterisation of materials is needed.

Based on an experimental setup, the measurement of the complete BRDF can be a solution. This requires measurements in all directions on the hemisphere covering the sample at a fixed angular pitch. For this, a system of articulated trays and arms carrying the optical sensors and the material sample is often required. Although relatively accurate, these systems have the disadvantage of requiring expensive sensors, such as a gonio-reflectometer [16] or a fibre spectrometer [17], and small samples of each material. Thus, the exhaustive characterisation of all the materials is difficult to envisage in a given environment.

In order to avoid this problem, an original approach is proposed in this article to determine the BRDF's parameters and so to characterise the materials. It uses a controlled environment with faces composed of distinct materials, whose reflective properties have to be characterised. A low-cost, standard and well-known Light Emitted Diode is added into the environment as well as a set of standard and known receivers (photodiodes), distributed in orientation and position. This approach first consists in measuring the optical power each receiver received, generating a reference signal. Secondly, it uses MCRT simulations feeding a global iterative optimization algorithm to converge the simulated and the reference signal. Starting from random data, at each iteration, the proposed optimization algorithm tries different sets of BRDF's parameters.

The novelty of this approach dedicated to OWC context lies in the combination of an optimization algorithm with an MCRT tool to adjust the BRDF's parameters, for the first time to our knowledge.

This paper is organised as follows. Section 2 presents the overall principle of the proposed method. Section 3 details the considered optimization algorithm. Section 4 provides initial results as a proof of concept of the proposed approach, on the basis of a purely numerical validation using a virtual measure obtained from simulation, and using three different test configurations. Finally conclusions and perspectives are provided in Section 5.

2 | PRINCIPLE'S OVERVIEW

The proposed system for optical characterisation of materials relies on the following three tools (*cf.* Figure 1):

- A measurement system of received optical power over a set of receivers.
- An optimization algorithm to estimate the unknown BRDFs' parameters.
- A lightwave propagation simulation software based on MCRT algorithms [18, 19].

Notice that the geometrical environment shown in Figure 1 is the Hospital room used in Section 4, but any other kind of indoor ones could be used instead.

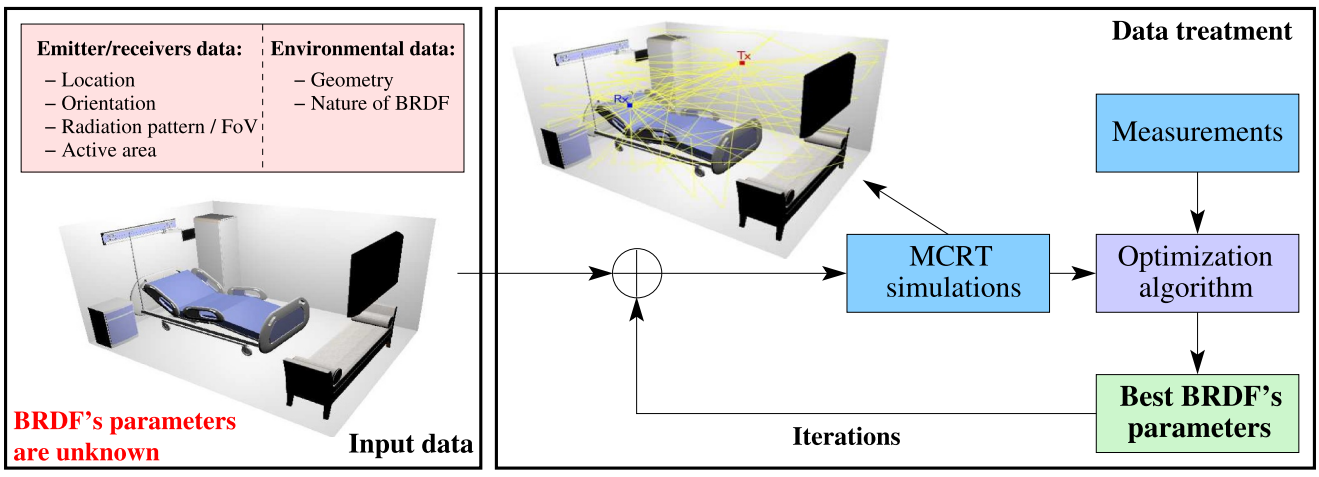

FIGURE 1 Optical characterisation system's principle.

The inputs of the system are: the sensors' characteristics, the 3D geometrical data of the propagation environment, the set of measurements realized at each of the receivers distributed in the real environment. The estimated parameters of the BRDFs are the outputs of the system.

Using MCRT simulations, the optimisation algorithm estimates the parameters of the searched BRDFs using a similarity evaluation between the simulated and measured signals. This evaluation relies on a specific function called *cost function*.

3 | OPTIMIZATION ALGORITHM

The aim of any optimization method is to evaluate the optimal set of parameters that optimises a cost function. In this paper's context, this set is the BRDF's parameters.

Many optimization techniques are proposed in the literature. Conventional methods relying on gradient descent require the derivative of the cost function. In our approach, the simulated signal is based on Monte Carlo methods and is therefore not given as an analytical expression. Hence, it is not possible to apply such a descent technique. Furthermore, the method must provide the global optimum of the cost function, but not a local one. Consequently, this paper uses a genetic algorithm, which is a stochastic optimization method reproducing natural selective without requiring the derivative of any function, and that explores the full parameter space. In similar application contexts, genetic algorithms have already shown their efficiency [20, 21] and their ability to converge towards the global optimum. The synoptic of the proposed genetic algorithm is presented in Figure 2.

The algorithm is randomly initialised with a list of elements, forming a first population. Each element is composed of all BRDF parameters. For each element of this population, an MCRT simulation is performed and then the cost function is evaluated. From these evaluations, a new population is created using three genetic operators: first selection, then crossing and finally mutation. The cost of these new elements is evaluated using a new MCRT simulation and the cost function. The former and new populations are then merged using a fourth operator, called fusion, which keeps only the best elements. The genetic algorithm iterates this cycle until a maximum number of iterations is reached or an acceptable solution is found.

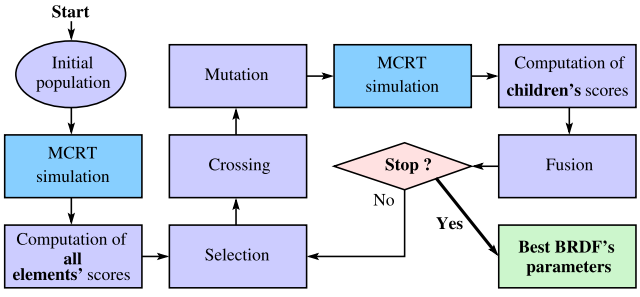

FIGURE 2 Proposed genetic algorithm's synoptic.

3.1 | Search domain

All the BRDFs considered in this paper are Lambertian, defined as follows:

$$R\left(x, \overrightarrow{\omega_i}, \overrightarrow{\omega_r}\right) = \frac{\rho}{\pi}, \tag{2}$$

where ρ is the albedo, x the reflection point, $\overrightarrow{\omega_i}$ and $\overrightarrow{\omega_r}$ the incident and reflection directions. The search domain corresponding to the range of possible albedo's values is [0,1].

3.2 | Initialisation

Any element of a population is a vector $(\rho_1, \ldots, \rho_n)$ having n coordinates, corresponding to the albedos of the n materials in the environment. Stratified sampling [22] is used to ensure a homogeneous distribution of elements in the element space. For example, with 6 different materials present in a controlled environment, then using 2 strata per ρ, the population is formed of $2^6 = 64$ elements, or $3^6 = 729$ elements using 3 strata.

3.3 | Evaluation of the cost function

The optimization algorithm relies on a criterion called the cost function to estimate the level of similarity between the reference (measured) signal and the simulated signal. This article uses two conventional criteria representing the two different families of similarity measurement between two signals:

- The Normalised Root Mean Square Error (*NRMSE*) is a measure of dispersion similar to the Root Mean Square Error, while facilitating the comparison between signals of different scales.
- The Pearson Correlation Coefficient (*PCC*) is a measure of the linear correlation between two sets of data.

3.3.1 | Normalised root mean square error

According to a given population, the global *NRMSE* is defined as follows:

$$NRMSE = \min_{i \in [1,\ldots,N_{Pop}]} \{NRMSE_i\} \tag{3}$$

where N_{Pop} is the population's size, and the error $NRMSE_i$ of the i^{th} element of the population is as follows:

$$NRMSE_i = \sqrt{\frac{1}{N_{Rx}} \sum_{j=1}^{N_{Rx}} \left(\frac{Sim_i(j) - Ref(j)}{Ref(j)}\right)^2}, \tag{4}$$

where Ref and Sim_i are, respectively, the reference and the simulated channel's gains (expressed in Watt) for each of the N_{Rx} receivers.

3.3.2 | Pearson correlation coefficient

According to a given population, the global *PCC* is defined as follows:

$$PCC = \max_{i \in [1,\ldots,N_{Pop}]} \{PCC_i\} \tag{5}$$

where the correlation coefficient PCC_i of the i^{th} element of the population is in the following:

$$PCC_i = \frac{\sum_{j=1}^{N_{Rx}} \Delta Sim_i(j) \Delta Ref(j)}{\sqrt{\sum_{j=1}^{N_{Rx}} (\Delta Sim_i(j))^2 \sum_{j=1}^{N_{Rx}} (\Delta Ref(j))^2}} \tag{6}$$

where $\Delta Sim_i(j) = Sim_i(j) - \overline{Sim_i}$, $\Delta Ref(j) = Ref(j) - \overline{Ref}$, $\overline{Sim_i}$ and $\overline{Ref}$ are the mean values of Sim_i and Ref, respectively, considering N_{R_x} receivers. PCC_i varies from −1 to 1; a value of 0 means no correlation, and −1 and +1 correspond to a complete linear correlation, negative and positive, respectively.

3.3.3 | From cost function to population's score

The optimization relies on a global score defined as follows:

$$N_{S_i} = \frac{S_i}{\max_{k \in [1,\ldots,N_{Pop}]} \{S_k\}}, \tag{7}$$

where S_i depends on the chosen cost function:

- Since *NRMSE* represents the dispersion measurement, the best score is obtained when it tends to 0. Hence, with *NRMSE*, the score is defined as follows:

$$S_i = \frac{1}{NRMSE_i}. \tag{8}$$

- On the contrary, *PCC* represents a correlation between two signals, obtained when PCC_i tends to 1. Hence, with *PCC*, the score is defined as follows:

$$S_i = PCC_i. \tag{9}$$

3.4 | Selection

The selection is described in Algorithm 1. In the current population (*Elements*), it consists in choosing a subset of $Nb_{Selected}$ elements (*Selected*). It corresponds to a given percentage (*SelectedPer*) of the population and is obtained in two steps. In the first one, to ensure that in the crossing step, a part of the most performing elements are considered, the set made of the *BestSelected* elements is selected, corresponding to the *BestSelectedPer* percentage of the best elements.

The second step tries to avoid convergence to a local minimum. It uses *simulated annealing* to ensure a significant probability $P(T)$ of selecting bad elements, especially during the first iterations. Using the image of temperature in physics T_j, the temperature reduces according to $T_j = T_1 . r^j$, where T_1 is the initial temperature and $0 < r < 1$ is the diminution rate. From T_1 and T_{nbIter} obtained at the last iteration *nbIter*, r is evaluated such that:

$$r = \sqrt[nbIter]{\frac{T_{nbIter}}{T_1}}, \qquad T_1 > T_{nbIter}. \tag{10}$$

Applying this principle, the probability $P(T)$ decreases as the number of iterations j increases (*cf.* Figure 3).

The population's diversity must be ensured over the generations in order to explore the element space as broadly as possible. The mutation and crossing operators help to assure this objective.

Algorithm 1 Selection algorithm.

$Selected = BestSelected$
while $Card(Selected) < Nb_{Selected}$ **do**
  $i \leftarrow$ uniform sampling into $Elements$
  computes N_{S_i} and $P(T) = e^{-(1-N_{S_i})/T}$
  $\xi \leftarrow$ uniform random sample in [0,1]
  if $\xi < P(T)$ **then**
    $Selected \leftarrow Selected + \{i\}$

Algorithm 2 Crossing algorithm.

$Children \leftarrow \{\}$
while $Card(Children) < N_{Pop}$ **do**
  p_1 uniform sampling into $Selected$
  p_2 uniform sampling into $Selected - \{p_1\}$
  foreach $k \in [1, n]$ **do**
    $(\rho_1, \rho_2) \leftarrow (p_1[k], p_2[k])$
    $\xi \leftarrow$ uniform random sample in [0,1]
    if $\xi < 0.5$ **then**
      $c[k] \leftarrow \rho_1$
    else
      $c[k] \leftarrow \rho_2$
  if $c \notin Children$ **then**
    $Children \leftarrow Children + \{c\}$

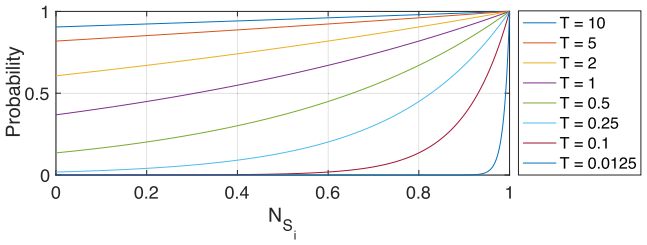

FIGURE 3 Element's choice probability versus its score and according to the temperature *T*.

3.5 | Crossing

Algorithm 2 describes the crossing step. From former population *Selected*, it uses some parents randomly chosen to generate new elements called children.

More precisely, the algorithm starts from a couple of parents $p_1 = (\rho_{1,1}, \rho_{2,1}, \ldots, \rho_{n,1})$ and $p_2 = (\rho_{1,2}, \rho_{2,2}, \ldots, \rho_{n,2})$ randomly chosen from *Selected*. Then, it generates a child $c = (\rho_1, \rho_2, \ldots, \rho_n)$, uniformly choosing between $\rho_{k,1}$ and $\rho_{k,2}$ for each ρ_k value. This process is repeated to produce N_{Pop} children. Notice that the same parents can be chosen many times during the whole crossing process.

Algorithm 3 Mutation algorithm of a child ρ_k value.

$\xi \leftarrow$ uniform random sample in [0,1]
if $\xi < P_M$ **then**
  $\rho_k \leftarrow$ DoMutation(ρ_k)

3.6 | Mutation

Algorithm 3 describes the mutation step. The objective is to potentially modify each child generated during the crossing step. For a given child, this algorithm modifies each of its BRDF' parameter ρ_k with probability P_M. When ρ_k has to be mutated, the algorithm does a Gaussian sampling using Algorithm 4. Gaussian sampling uses the former ρ_k as mean value, while its standard deviation σ is a follows:

$$\sigma = \frac{1}{4}.\left(1 - \frac{j-1}{nbIter}\right)^b, \tag{11}$$

where j is the number of iterations of the optimization algorithm, and b is an empirically fixed global parameter. The principle is to ensure a good exploration of the space of elements during the first iterations, then to reduce the size of this space as the elements get closer to the solution. In practice, this consists in progressively reducing σ so as to reduce the average changes brought about by the mutations, as the iterations progress.

It is worth noting a problem that can arise with this mutation method: sampling can produce a new ρ_k outside the [0,1] albedo space. This problem is illustrated in Figure 4 with two examples where the ρ_k parameters of values 0.1 and 0.9 have to be mutated with $\sigma = 0.2$: in both cases, the probability of sampling a ρ'_k value lower than 0 and higher than 1, respectively, is quite high. To overcome this problem, a rejection sampling mechanism is used to restrict the sampled value ρ_k to [0…1]. This method guarantees a correct Gaussian probability distribution.

3.7 | Fusion

From the population of iteration j and the new population composed of the elements generated after mutation, the fusion consists in generating the elements of the population used at iteration $j + 1$. The aim is to retain the N_{Pop} best elements of both populations. To do so, this step first consists in evaluating the scores of the elements of the population generated after the mutation step. This is done by estimating the channel gain for each receiver using an MCRT simulation and then calculating their score using the cost function (see Figure 2). Then, the elements of the two populations are merged and sorted by decreasing order of scores. Finally, the first N_{Pop} are kept, corresponding to the best N_{Pop}.

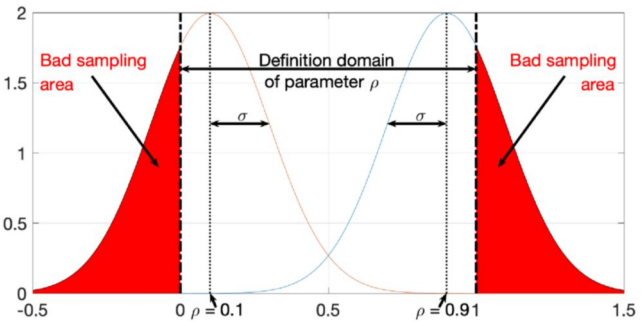

FIGURE 4 Sampling outside the albedo's definition domain.

3.8 | Stop criteria

Two criteria can be taken into account to stop this optimisation algorithm. The first is based on an accuracy threshold: the algorithm is stopped when the best element reaches a target value of the cost function. The second criterion consists in stopping the algorithm after a fixed maximum number of iterations. We only consider the latter criterion to theoretically validate the algorithm in the rest of this paper.

Algorithm 4 DoMutation(ρ_k).

do
  $\rho'_k \leftarrow$ GaussianRandomSampling(ρ_k, σ)
while $(\rho'_k < 0) \parallel (\rho'_k > 1)$;
$\rho_k \leftarrow \rho'_k$

4 | ALGORITHM VALIDATION

This section aims at validating the optimization algorithm proposed in this paper. This algorithm is based on a signal measured in an experimental environment and on simulations performed in a virtual environment. The latter must be close enough to the experimental environment to obtain the same signal as the measured one. Hence, the validation relies onto two different criteria:

1) The algorithm converges: does the simulation signal converge to the measured one?

2) The algorithm converges to the global optimum: do the found parameters correspond to the real ones?

Let us recall that the parameters, we search are BRDFs of some materials (albedo).

To do this validation, we need to know all the parameters from the experimental setup, including the searched ones. The sole method to obtain these physical parameters is to measure them. Unfortunately, the physical measurement of any physical parameter can be a challenge especially for the searched ones (albedo), and at best can be done with a margin of error. What is the impact of these uncertainties on the optimization algorithm convergence? In case of convergence, does the algorithm converge to a global optimum or a local one?

To overcome these problems, we propose *to simulate the measurement*, such that all the parameters involved in the measurement are fully known and controlled, in order to be able to discuss the validity of the optimisation algorithm accurately. In the following, this simulated measurement is called the *virtual measurement*.

Our validation is then based on the four following different configurations, three with a same but simple geometrical environment, and the last one with a more complex and realistic geometry.

- *Exact configuration*: it is made such that the input data of both the *virtual measurement* and the optimization algorithm are perfectly known. The virtual environment data are described in Figure 1, including the physical parameters of the sensors, their location *etc.*
- *Erroneous configuration 1*: starting from the exact configuration, it introduces a controlled error onto the radiated power of the transceiver.
- *Erroneous configuration 2*: starting from the exact configuration, it introduces a controlled error onto the transmitter's orientation.
- *Hospital configuration*: a more complex geometrical environment with pieces of furniture like a bed, sofa, wardrobe, etc., and hence more BRDF to fit.

4.1 | Simulation configurations

The *exact configuration* is depicted in Figure 5 and Table 1. Walls, ceiling and floor are made of specific materials, which have to be characterised by the genetic algorithm. The reference signal corresponds to the optical power, which would be measured on a set of receivers distributed inside the room. As previously mentioned, in this first approach, we consider a purely numerical validation by replacing measurement data with *virtual measurement* based on our MCRT tool by considering a maximum of 3 successive reflections and the materials given in Table 1.

To help the genetic algorithm, the reference signal has to be significantly impacted by all the materials composing the environment. To achieve this, we consider a set of receivers whose respective locations tend to be uniformly distributed over a sphere centred on a reference location indicated in Table 1. They are oriented according to the radius of the sphere, fixed to 20 cm to set the receivers' locations. However, a conventional random uniform sampling leads to a concentration of receivers on given zones of the sphere's surface, while some other areas are empty of point (cf. Figure 6a for 128 receivers). If more receivers point to a specific zone, and that few ones (maybe 0) point to other zones, the impact on the reference signal of the corresponding materials will be high and low respectively. Consequently, it will be difficult for the genetic algorithm to estimate well the material parameters of surfaces having low impact on both reference and simulated signals. To avoid this problem, we consider the deterministic Fibonacci [23] sampling method, which always provides the same distribution of locations onto the sphere, for a given number of samples, while minimising the discrepancy, that is, the maximum distance between any couple of receivers to the set of locations (cf. Figure 6b for 128 receivers). In this study, the impact of this parameter onto the genetic algorithm is analysed by considering between 1 and 20 receivers.

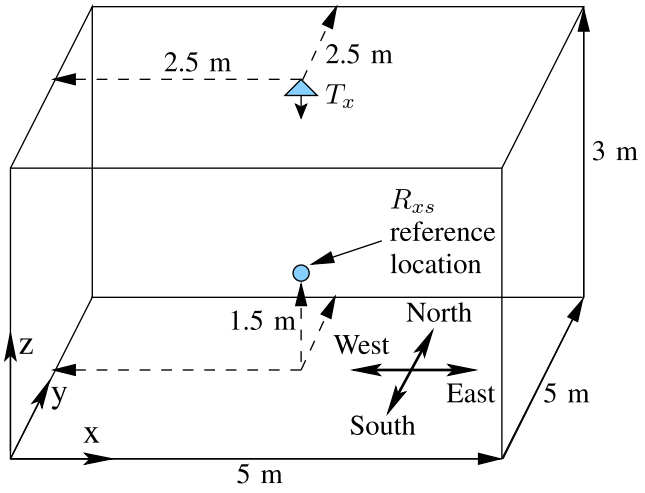

FIGURE 5 Simulation environment for the first three configurations.

TABLE 1 Parameters of the exact configuration propagation environment.

Parameters	Values
Room size	5 × 5 × 3 m
Surfaces' BRDFs model	Lambertian
T_x location	(2.5, 2.5, 2.99)
T_x orientation	(0, 0, −1)
T_x power	1 W (normalised)
T_x geometrical shape/area	Circular/1 cm^2
R_{xs} reference location	(2.5, 2.5, 1.5)
R_{xs} geometrical shape/area	Circular/1 cm^2
FoV of the receivers	60°
ρ of ceiling/floor	0.8/0.3
ρ of east/west/south/north walls	0.4/0.7/0.5/0.9

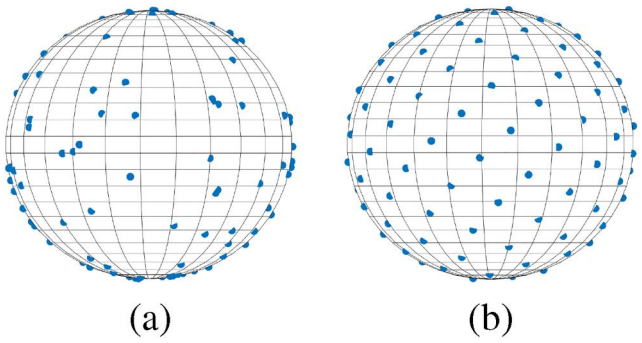

FIGURE 6 Example of distribution of 128 receivers from (a) the classical random uniform sampling and (b) the Fibonacci sampling.

Previous works have highlighted the bad knowledge of the emitted optical irradiance of conventional LEDs, which can vary by a factor from 2 to 5 due to differences in manufacturing processes [15]. To analyse its corresponding impact onto the genetic algorithm convergence to the global optimum, we propose the *Erroneous configuration 1*: based on the *Exact configuration*, it multiplies its emitted optical irradiance by a factor of 2.

Another parameter that is difficult to measure is the orientation of sensors. To quantify its impact on the genetic algorithm convergence, the *Erroneous configuration 2* modifies the orientation of the transmitter by 10°, starting from the *Exact configuration*. More precisely, its orientation is given by the vector $\{0, -0.174, -0.985\}$.

While the first three configurations share the same geometry and BRDF, to explore the robustness of the method in more complex scenarios, we use a fourth configuration with a different and more complex environment. This configuration is called *Hospital configuration* and is shown in Figure 1. It contains 8 different BRDF, and some pieces of furniture: a bed with a mattress and a bed structure, a sofa, a wardrobe, a bedside table, a TV, an oxygen block up to the bed and of course the room. Each of these elements has one corresponding BRDF (*cf.* Table 2).

TABLE 2 Parameters of the hospital configuration propagation environment.

Parameters	Values
Room size	2.83 × 3.79 × 2.07 m
Surfaces' BRDFs model	Lambertian
T_x location	(1.3, 2.0, 2.0)
T_x orientation	(0, 0, −1)
T_x power	1 W (normalised)
T_x geometrical shape/area	Circular/1 cm^2
R_{xs} reference location	(1.3, 1.3, 1.4)
R_{xs} geometrical shape/area	Circular/1 cm^2
FoV of the receivers	60°
ρ of room (ceiling/floor/east/west/south/north walls)	0.7
ρ of wardrobe	0.6
ρ of mattress	0.4
ρ of sofa	0.3
ρ of TV	0.2
ρ of bed structure	0.9
ρ of oxygen block	0.5
ρ of bed side table	0.65

4.2 | Genetic algorithm configuration

The results presented in Section 4.3 have been obtained by configuring the genetic algorithm as follows:

- Global parameters: $nbIter = 100$, $N_{Pop} = 64$.
- Selection: $BestSelectedPer = 5\%$, $SelectedPer = 50\%$, $Nb_{Selected} = SelectedPer \cdot N_{Pop}$, $T_1 = 10$, $T_{nbIter} = 0.1$.
- Mutation: $P_M = 0.5$, $b = 1$.

4.3 | Results and discussion

The proposed optimization algorithm is stochastic since it depends on the initial population and on the numerous random sampling needed for the selection/crossing/mutation steps. Then, every run leads to different initial populations and different crossed/mutated ρ values. Nevertheless, all these runs should tend to the same result when the iteration number tends to infinity. This results in the maximum score we can expect for the given input parameters. Let us recall that the score depends on the cost function that tends to zero using *NRMSE* and 1 using *PCC*.

This section presents the simulation results for the four introduced configurations, showing the evolution of both the cost functions (excepting Hospital configuration that uses PCC only) and the best population's element according to the number of considered receivers and for 10 runs.

4.3.1 | Exact configuration

Figures 7 and 8 show the evolution of the cost functions *NRMSE* and *PCC* versus the iteration numbers for 10 different runs. The curves tend to 0 and 1, respectively, indicating that the genetic algorithm seems to converge as previously mentioned.

To check if the algorithm tends to the global optimum, we statistically compare the ρ values of the best element after the 100 iterations to the objective ones by computing the mean and standard deviation of the ρ values over the 10 runs. Figures 9 and 10 show these data (crosses and vertical lines are the mean and the standard deviation values respectively) over 10 runs according to the number of considered receivers,

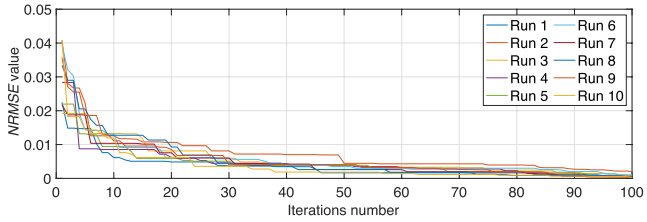

FIGURE 7 Evolution of the best value of the cost function as a function of the number of iterations (*Exact configuration–NRMSE*).

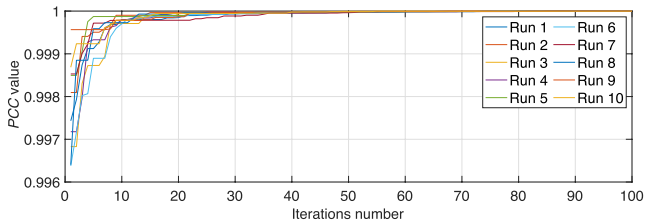

FIGURE 8 Evolution of the best value of the cost function as a function of the number of iterations (*Exact configuration–PCC*).

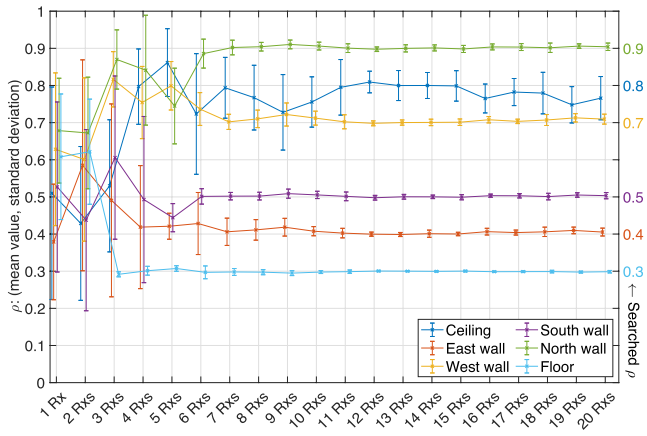

FIGURE 9 Performance statistics according to the number of receivers (*Exact configuration–NRMSE*).

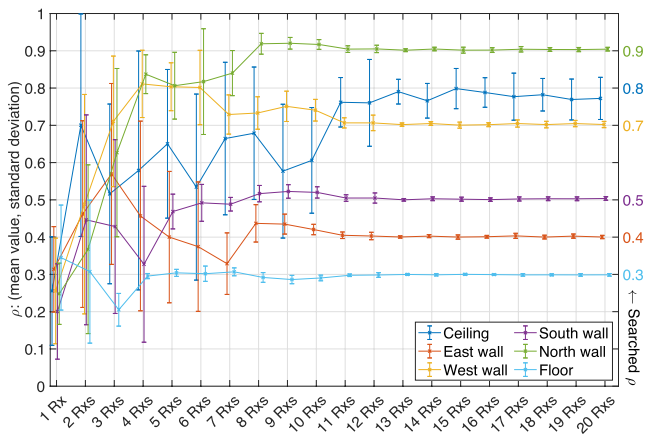

FIGURE 10 Performance statistics according to the number of receivers (*Exact configuration–PCC*).

considering *NRMSE* and *PCC* cost function, respectively. From these curves, we can conclude that the ρ estimation is all the more accurate when the number of receivers is high. Whatever the cost function, a number of 11 receivers seem to be sufficient to well estimate the 6 ρ in terms of mean values. The algorithm's stability is also quite good since the standard deviations are weak, except for the ceiling. The transmitter being on the ceiling and radiating towards the floor, the contributions reflected on the ceiling need at least two reflections, while they need only one reflection for the floor and the walls. Consequently, they carry less power when reflecting onto the ceiling compared to the other surfaces, and therefore, should have a smaller impact on the cost function, regardless of the ceiling's ρ value.

Let us check this hypothesis by analysing Table 3 for *NRMSE*. It shows the evolution of the cost function according to extreme possible ρ values (0.1 and 0.9) for the ceiling and the east wall, the other surfaces'ρ being fixed to expected values. The cost function is first computed (row 1) considering the reference signal (*Ref*) obtained for the ceiling's ρ value of 0.8 (cf. Table 1). In this configuration, the maximum cost function's values (in red) are 0.082 and 0.171 for the ceiling and the east wall, respectively, indicating a 2 times lower impact for the ceiling, as expected. The second row of Table 3 shows the cost function's values obtained for a reference signal computed considering a ceiling's ρ value of 0.2. In this configuration, the maximum cost functions' values (in red) are 0.092 and 0.246 for the ceiling and the east wall respectively, that is, a 2.5 times lower impact for the ceiling. These results confirm that the genetic algorithm has more difficulty in properly estimating the ceiling's ρ value because of its lower impact onto the cost function due to the geometrical configuration.

4.3.2 | Erroneous configuration 1

The evolution of the *NRMSE* cost function presented in Figure 11 is different from that observed for the *Exact configuration*. While the *NRMSE* value still decreases according to the number of iterations, it seems to reach a limit of about 1.62, far from the optimal value of 0, indicating that the genetic algorithm has failed to converge. This analysis is confirmed by Figure 12, which shows the reference signal (*i.e.* the *virtual measurement*) compared to the estimated powers received on each of the receivers over the 10 runs of the genetic algorithm; theses curves are significantly different.

Consequently, the statistics of the ρ values of the best element after 100 iterations are shown in Figure 13, highlighting the non-convergence of the algorithm: the

TABLE 3 Surfaces' impacts on the *NRMSE* cost function.

	Ceiling's ρ		East wall's ρ	
	0.1	**0.9**	**0.1**	**0.9**
Reference ceiling's $\rho = 0.8$	0.082	0.012	0.099	0.171
Reference ceiling's $\rho = 0.2$	0.013	0.092	0.076	0.246

optimization algorithm visibly leads to a local optimum but not to the global one. It can be observed from Figure 12 some peaks and troughs. For the troughs, the impact of albedo change on the *NRMSE* is limited due to power close to 0, while it could be important for peaks. Hence, *NRMSE* privileges the peaks.

Conversely, the use of the *PCC* cost function keeps the algorithm converging well as indicated by Figure 14 where *PCC* values tend to 1. Indeed, Figure 15 shows that the reference and estimated signals are almost superposed. This is confirmed by the statistics of estimated ρ values depicted in Figure 16: they are close to the objective albedos from 11 receivers.

4.3.3 | Erroneous configuration 2

In this configuration, the orientation of the transmitter is {0, −0.174, −0.985}, corresponding to a 10° change. Figures 17 and 18 seem to both indicate a good convergence with cost function values tending to 0 and 1, respectively. This first observation is confirmed by the comparison between the reference signal and the estimated ones based on *NRMSE* and

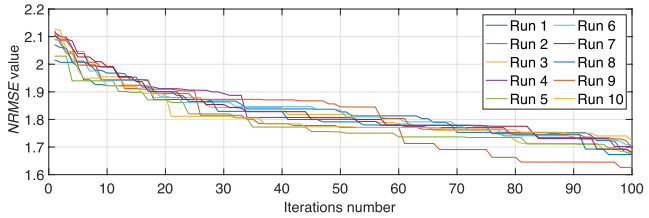

FIGURE 11 Evolution of the best value of the cost function as a function of the number of iterations (*Erroneous configuration 1–NRMSE*).

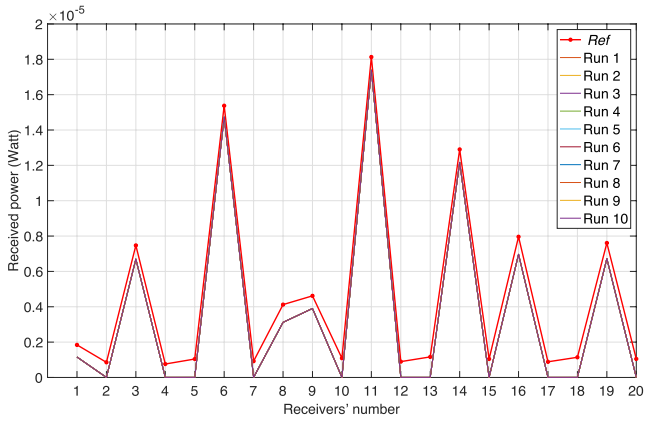

FIGURE 12 Reference signal versus simulated signal (*Erroneous configuration 1–NRMSE*).

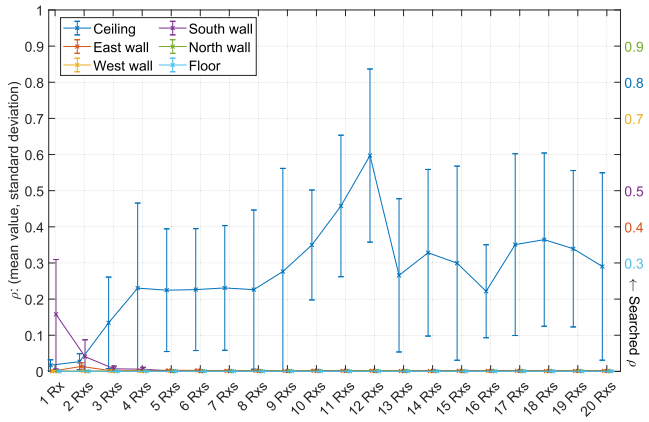

FIGURE 13 Performance statistics according to the number of receivers (*Erroneous configuration 1–NRMSE*).

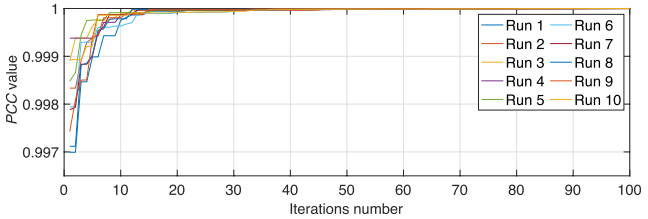

FIGURE 14 Evolution of the best value of the cost function as a function of the number of iterations (*Erroneous configuration 1–PCC*).

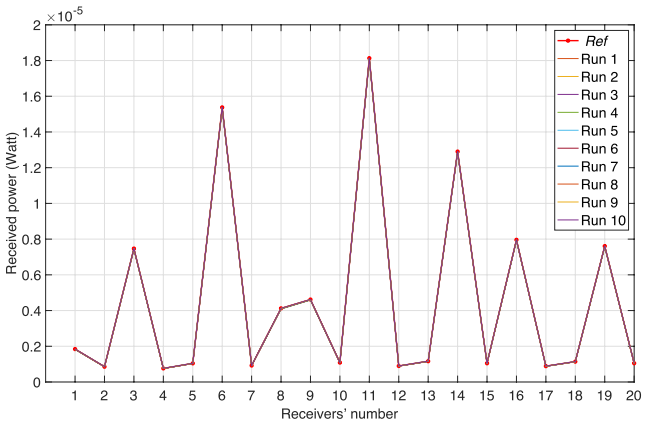

FIGURE 15 Reference signal versus simulated signal (*Erroneous configuration 1–PCC*).

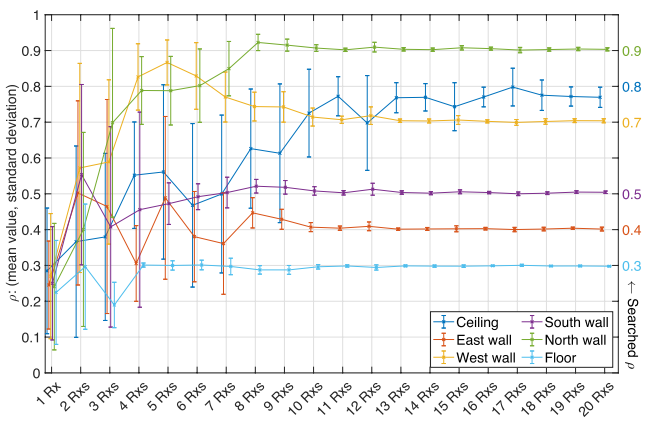

FIGURE 16 Performance statistics according to the number of receivers (*Erroneous configuration 1–PCC*).

PCC cost functions, depicted in Figures 19 and 20; these curves appear to be well overlapped.

Nevertheless, the statistical analysis of the ρ values of the best element after 100 iterations, shown in Figure 21 for *NRMSE* and Figure 22 for *PCC*, indicates that in both cases, the genetic algorithm converged to a local minimum, characterised by a wrong set of estimated albedos.

4.3.4 | Hospital configuration

Based on the previous results, we focus on the *PCC* cost function for this more realistic and complex configuration. Presenting the evolution of the *PCC* values over the iterations, Figure 23 still shows a good convergence of the cost function that tends to 1. This result is confirmed by Figure 24 that shows a very good overlapping between the reference signal and the estimated one.

Finally, Figure 25 allows a more in-depth analysis of the performance of our method by showing the evolution of the estimated albedo statistics over the considered number of

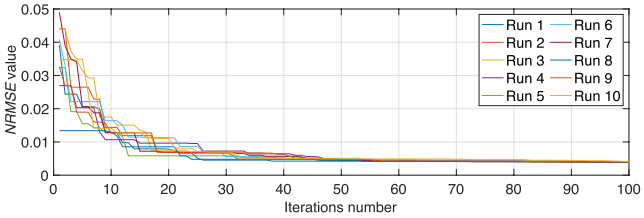

FIGURE 17 Evolution of the best value of the cost function as a function of the number of iterations (*Erroneous configuration 2–NRMSE*).

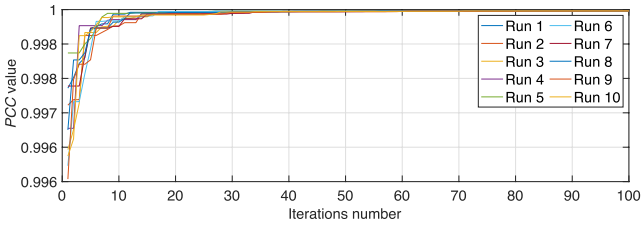

FIGURE 18 Evolution of the best value of the cost function as a function of the number of iterations (*Erroneous configuration 2–PCC*).

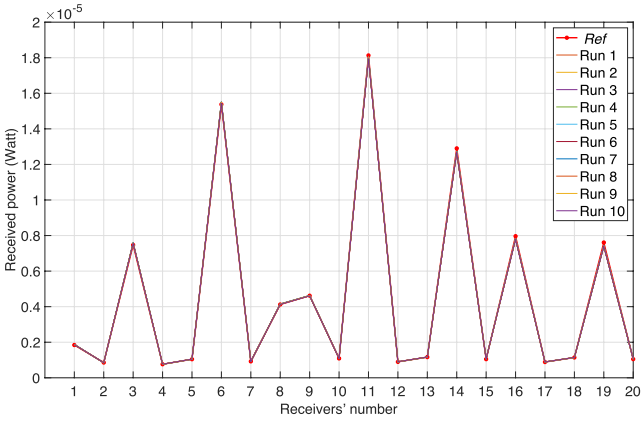

FIGURE 19 Reference signal versus simulated signal (*Erroneous configuration 2–NRMSE*).

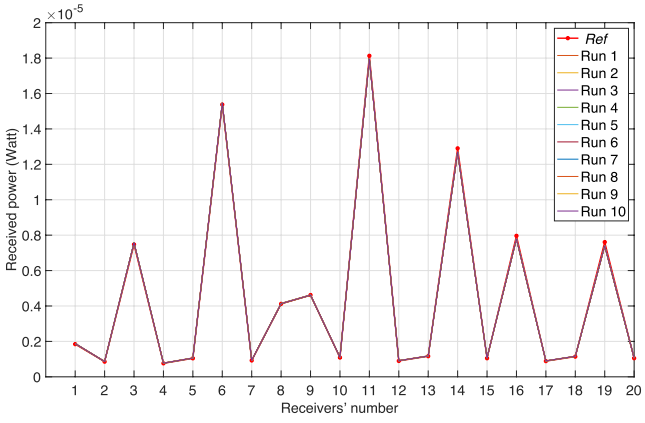

FIGURE 20 Reference signal versus simulated signal (*Erroneous configuration 2–PCC*).

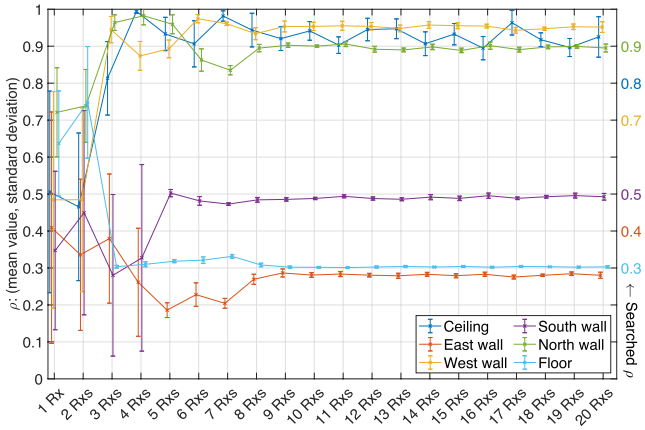

FIGURE 21 Performance statistics according to the number of receivers (*Erroneous configuration 2–NRMSE*).

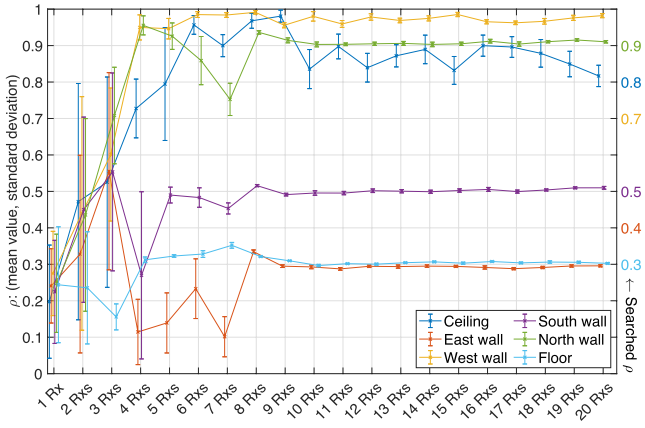

FIGURE 22 Performance statistics according to the number of receivers (*Erroneous configuration 2–PCC*).

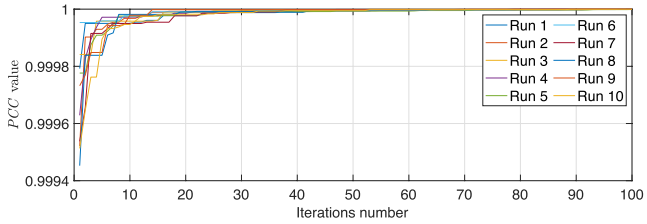

FIGURE 23 Evolution of the best value of the cost function as a function of the number of iterations (*Hospital configuration–PCC*).

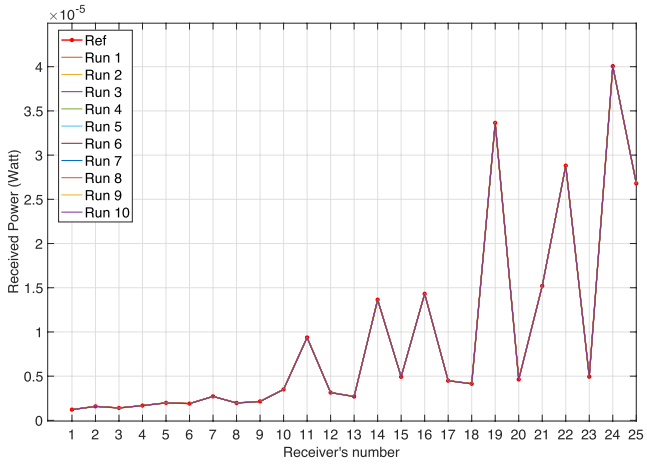

FIGURE 24 Reference signal versus simulated signal (*Hospital configuration–PCC*).

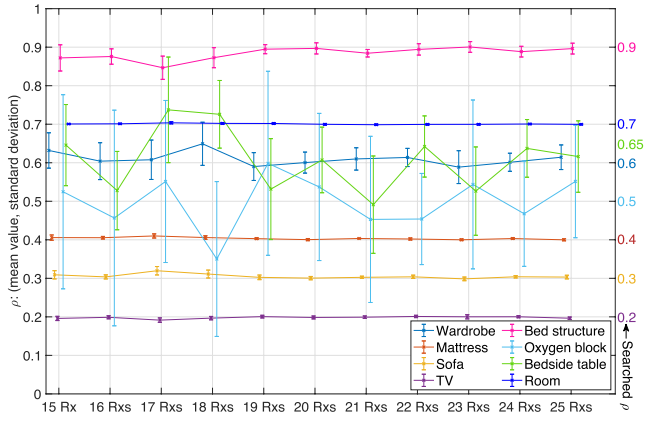

FIGURE 25 Performance statistics according to the number of receivers (*Hospital configuration–PCC*).

receivers. The same observations as for the previous configurations can be made again. First of all, most of the albedos can be correctly estimated (room, TV, mattress, sofa and bed structure). However, some albedos are more difficult to obtain and have a large standard deviation: those of the bedside table, the oxygen block, and to a lesser extent, the wardrobe. As for the ceiling in the previous configurations, it can be observed that these pieces of furniture are either small compared to the propagation environment or far away or poorly oriented from the sensors. Their influence on the received optical power is therefore imperceptible.

4.4 | Discussion

With a perfect knowledge of all the input data, the *Exact configuration* proposed in Section 1 has shown that the genetic algorithm is able of converging well towards the global optimum with the two considered cost functions, namely, *NRMSE* and *PCC*. Consequently, the albedo of each material composing the experimental environment is well identified, which validates the algorithm. Unfortunately, the precise knowledge of all these input data is a difficult task to guarantee. It is therefore important to analyse the impact of erroneous input data onto the ability of the genetic algorithm to find the correct values of the searched parameters, that is, the albedos.

Considering an erroneous transmitted optical power, Section 2 has shown that using the *NRMSE* cost function does not allow the genetic algorithm to converge, because the received power is limited to positive values. Conversely, with the *PCC* cost function, not only the genetic algorithm always converges, but also it converges to the global optimum. Indeed, by using *PCC*, the algorithm searches for a curve with a similar shape to the reference signal, whatever its mean value. Hence, *PCC* is a more robust cost function with respect to the uncertainty of this type of input data.

Section 3 analysed the impact of a wrong orientation of the transmitter. It showed that, whatever the cost function used, it is impossible for the genetic algorithm to find the global optimum: it converges to a local minimum, leading to an erroneous set of albedos. To solve this configuration, it would be necessary to introduce the orientation of the transmitter as a new parameter sought in the genetic algorithm, but at the cost of an increase in complexity. Another way would be to improve the experimental setup to ensure a good parameterisation of the optimization algorithm.

Finally, Section 4 has illustrated the behaviour of the proposed method in the case of a more complex and realistic propagation environment, that is, the Hospital configuration. As for the simple previous environment, most of the materials are well estimated, except the one of furniture having a small area compared to the environment dimensions, or being far from the sensors, leading to a weak impact on the received optical power.

A further improvement for the optical characterisation of certain materials, such as the ceiling in the *Exact configuration*, but also more generally for the characterisation of a large number of materials composing a realistic environment (as Hospital environment), would be to use more receivers and transmitters distributed in the environment, so that each material has a significant impact on the reference/measured signals. This solution should also help to characterise materials whose reflection behaviour follows a more complex BRDF model characterised by several parameters, for example, Phong

[19]. Both types of sensors could be mapped onto different 3D printed spheres distributed in the environment, similar to our first prototype shown in Figure 26.

This experimental setup is realised as follows. Each sensor is mounted on a rectangular printed circuit board (PCB). The 3D model of the sphere carrying the sensors is first designed under a 3D modelling software like Blender. The positions of the sensors are calculated by the Fibonacci method presented in Section 4.1. At these positions, the 3D model of the sphere is drilled in order to insert the PCBs carrying the sensors. These PCBs are screwed into the thickness of the 3D printed sphere so that the active surface of the sensor is flush with the outer surface of the sphere.

5 | CONCLUSION

This paper has proposed a new approach for optical characterisation of materials composing indoor environment, based first on measurement using a simple and low-cost setup, and then on numerical simulation from an MCRT tool, feeding a genetic algorithm capable of fitting the simulated data to the measured ones. This paper fully describes the different steps of this algorithm, including two different cost functions to find the optimal materials. These cost functions are the *NRMSE* and the *PCC*.

To ensure that the input data are perfectly known, so that the algorithm can be discussed accurately, this paper provided a proof of concept by replacing measured data with simulated data, leading to a purely numerical validation process. The results showed that the optimization algorithm performs well with these two cost functions, in the conditions of the proposed environments: correct choice of BRDF models and significant influence of each material onto the received optical power.

Secondly, this paper attempted to add a controlled error in the input data for two particularly difficult to acquire data: it first considered an erroneous radiated power, and second an erroneous orientation of the transmitter. For the first case, *NRMSE* failed to obtain the right albedos, while *PCC* still provides good results. For the second case, both cost functions did not give the expected albedos, indicating that a good measurement of the sensors' orientation should be guaranteed or that a rotation matrix applied to the sensors should be added to the parameters sought for the optimization.

Finally, this paper explores a more complex environment with more materials and a more complex geometry with some pieces of furniture. The conclusions drawn from the three previous configurations are still valid: a good estimate of BRDFs having a direct impact on the received optical power and a poor estimate for the other BRDFs' albedo. A direct extension of this work can be to fix the obtained BRDF having a low standard deviation, then move the receivers closer to the not yet characterized materials to perform a new measurement, and so on until all materials are correctly characterised.

There exist many other future works, such as implementing the measurement setup, studying the case of more complex BRDFs, testing other cost functions and exploring the impact of different parameters of the algorithm.

Finally, it will be necessary to study this method with real measurements, not just virtual, in order to validate it as a valid and inexpensive method for characterizing materials in OWC systems.

(a)

(b)

FIGURE 26 Sensors support: (a) 3D model and (b) 3D printed prototype.

AUTHOR CONTRIBUTIONS

Pierre Combeau: Paper writing, code writing, and experimentation. **Lilian Aveneau**: Paper writing, code writing, and experimentation. **Pierre Thuillier Le Gac**: Code writing and experimentation. **Ruqin Xiao**: Code writing, experimentation.

ACKNOWLEDGEMENTS

This work was supported by both the European Union under Grant agreement 737645, through the Cleansky2 H2020 project titled Aircraft Light Communication (ALC), and the Nouvelle-Aquitaine Region under Grant agreement 8554510, through the project titled Modélisation Avancée du Canal de propagation OPTique sans fil (MACOPT).

CONFLICT OF INTEREST STATEMENT

The authors affirm that they have no conflict of interest.

DATA AVAILABILITY STATEMENT

Data sharing is not applicable to this article as no new data were created or analysed in this study.

ORCID

Pierre Combeau https://orcid.org/0000-0002-8226-1145

REFERENCES

1. Arnon, S. (ed.) Visible light communication, 1st ed. Cambridge University Press (2015)
2. Dimitrov, S., Haas, H.: Principles of LED Light Communications towards Networked Li-Fi. Cambridge University Press (2015)
3. Ghassemlooy, Z., Popoola, W.O., Rajbhandari, S.: Optical Wireless Communications - System and Channel Modelling with Matlab. CRC Press (2012)
4. Miramirkhani, F., Uysal, M.: Channel modeling and characterization for visible light communications. IEEE Photon. J. 7(6), 1–16 (2015). https://doi.org/10.1109/jphot.2015.2504238
5. Barry, J.R., et al.: Simulation of multipath impulse response for indoor wireless optical channels. IEEE J. Sel. Area. Commun. 11(3), 367–379 (1993). https://doi.org/10.1109/49.219552
6. Pérez Rodríguez, S., et al.: Simulation of impulse response for indoor visible light communications using 3D CAD models. EURASIP J. Wirel. Commun. Netw. 2013(1), 7 (2013). https://doi.org/10.1186/1687-1499-2013-7
7. Kavehrad, M., Sakib Chowdhury, M.I., Zhou, Z.: Short Range Optical Wireless. John Wiley and Sons Ltd (2015)
8. Mermet-Lyaudoz, R., et al.: Multiscale simulation for visible light communication using perovskite metasurface. In: 2021 17th International Symposium on Wireless Communication Systems (ISWCS). IEEE (2021)
9. Pharr, M., Humphreys, G.: Physically Based Rendering: From Theory to Implementation. Morgan Kaufmann (2010)
10. Kahn, J.M., Krause, W.J., Carruthers, J.B.: Experimental characterization of non-directed indoor infrared channels. IEEE Trans. Commun. 43(2/3/4), 1613–1623 (1995). https://doi.org/10.1109/26.380210
11. Lomba, C.R., Valadas, R.T., de Oliveira Duarte, A.M.: Experimental characterisation and modelling of the reflection of infrared signals on indoor surfaces. IEE Proc. Optoelectron. 145(3), 191–197 (1998). https://doi.org/10.1049/ip-opt:19982020
12. Rodriguez Perez, S., et al.: Reflection model for calculation of the impulse response on IR-wireless indoor channels using ray-tracing algorithm. Microw. Opt. Technol. Lett. 32(4), 296–300 (2002). https://doi.org/10.1002/mop.10159
13. Lee, K., Park, H., Barry, J.R.: Indoor channel characteristics for visible light communications. IEEE Commun. Lett. 15(2), 217–219 (2011). https://doi.org/10.1109/lcomm.2011.010411.101945
14. Behlouli, A., et al.: Impact of physical and geometrical parameters on visible light communication links. In: Advances in Wireless and Optical Communications (RTUWO), Riga, Latvia. IEEE (2017)
15. Combeau, P., et al.: Optical wireless channel simulation for communications inside aircraft cockpits. J. Lightwave Technol. 38(20), 5635–5648 (2020). https://doi.org/10.1109/jlt.2020.3003989
16. Belcour, L., et al.: Bidirectional reflectance distribution function measurements and analysis of retroreflective materials. J. Opt. Soc. Am. 31(12), 2561 (2014). https://doi.org/10.1364/josaa.31.002561
17. Wang, H., Zhang, W., Dong, A.: Measurement and modeling of bidirectional reflectance distribution function (BRDF) on material surface. Measurement 46(9), 3654–3661 (2013). https://doi.org/10.1016/j.measurement.2013.07.008
18. Behlouli, A., et al.: Efficient simulation of optical wireless channel application to WBANs with MISO link. Procedia Comput. Sci. 40(0), 190–197 (2014). https://doi.org/10.1016/j.procs.2014.12.027. Fourth International Conference on Selected Topics in Mobile and Wireless Networking (MoWNet'2014)
19. Behlouli, A., Combeau, P., Aveneau, L.: MCMC methods for realistic indoor wireless optical channels simulation. IEEE/OSA J. Lightwave Technol. 35(9), 1575–1587 (2017). https://doi.org/10.1109/jlt.2017.2662939
20. Infantolino, J.M.K., Barney, M.J., Haupt, R.L.: Using a genetic algorithm to determine an optimal position for an antenna mounted on a platform. In: IEEE Military Communications Conference, Boston, MA, USA. IEEE (2009)
21. Combeau, P., et al.: A numerical simulation system for mobile telephony base station EMF exposure using smartphones as probes and a genetic algorithm to improve accuracy. Prog. Electromagn. Res. B 87, 111–129 (2020). https://doi.org/10.2528/pierb20020404
22. Särndal, C.E., Swensson, B., Wretman, J.: Model Assisted Survey Sampling. Springer, New York (2003)
23. González, Á.: Measurement of areas on a sphere using Fibonacci and latitude–longitude lattices. Math. Geosci. 42(1), 49–64 (2009). https://doi.org/10.1007/s11004-009-9257-x

How to cite this article: Combeau, P., et al.: Material characterisation for optical wireless communication combining measurement and Monte Carlo simulations. IET Optoelectron. 17(4), 149–161 (2023). https://doi.org/10.1049/ote2.12098